NUREG/CR-6603
SAND98-0419
RW

Characterization of Retardation Mechanisms in Soil

Manuscript Completed: January 1998
Date Published: April 1998

Prepared by
H. R. Westrich, P. V. Brady, R. T. Cygan, S. E. Gruenhagen, H. L. Anderson, SNL
K. L. Nagy*

Sandia National Laboratories
Albuquerque, NM 87185-0750

*University of Colorado
Boulder, CO

E. O'Donnell, NRC Project Manager

Prepared for
Waste Management Branch
Division of Regulatory Applications
Office of Nuclear Regulatory Research
U. S. Nuclear Regulatory Commission
Washington, DC 20555-0001
NRC Job Code B6608

Abstract

Realistic performance assessment of low-level radioactive waste sites is dependent upon our understanding of the transport and retardation of radionuclides in soils under a variety of geochemical conditions. Improved fate and transport codes should include a mechanistic model of radionuclide retardation so as to minimize uncertainties. We have investigated metal sorption (Cs^+, Sr^{2+}, and Ba^{2+}) on a simple clay mineral (kaolinite) to better understand the geochemical interactions of common soil minerals with contaminated groundwaters. Our studies include detailed characterizations of kaolinite surfaces and sorption sites, experimental adsorption measurements, surface complexation modeling, and theoretical simulations of cation sorption. Spectroscopic analyses of Cs-exchanged samples show that Cs is sorbed at mineral surfaces and at the interlayer site of smectite clays and on edge and basal sites of kaolinite. Atomic Force Microscopic examination of kaolinite crystallites suggests that edges comprise from 10 to 50% of its measured surface area. Proton adsorption isotherms for kaolinite and molecular modeling results show that aluminol edge binding sites are more reactive at typical soil pH than silanol edge sites, and are the most likely sites for metal sorption on kaolinite in natural solutions. Relative metal binding strengths decrease from Ba^{2+} to Sr^{2+} to Cs^+, with some portion sorbed on both kaolinite edges and basal surfaces. Some Cs^+ also appears to be irreversibly sorbed on all sites. Molecular dynamics simulations suggest that Cs^+ is sorbed at aluminol (010) edge sites as an inner-sphere complex and weakly sorbed as an outer-sphere complex on (001) basal surfaces. The first, all-atom structure energy minimization for kaolinite was completed, and calculated cell dimensions, bond lengths and bond angles agree very well with observed values. These results provide the validation for accurate descriptions of more complex structures that will be used in simulations of metal sorption onto realistic clay minerals. Recent measurements and characterization of Sr^{2+} and Ba^{2+} sorption onto montmorillonite clay indicate that montmorillonite metal binding strengths are similar to those seen for kaolinite. In contrast to kaolinite sorption, the basal plane residual charge in smectite clays greatly influences metal sorption. On the other hand, phase transformation kinetics (ferrihydrite to goethite) may be a more important control over metal sorption and desorption from Fe-oxides/hydroxides. These measurements are being extended and will be interpreted in light of new atomistic simulations. These results provide a basis for understanding and predicting metal sorption onto kaolinite, and a framework for characterizing sorption processes on more complex soil minerals.

Contents

List of Figures

Table

Disclaimer:

NUREG\CR-6603

Is not a substitute for NRC regulations, and compliance is not required. The approaches , end or methods described in the NUREG\CR are provided for information only. Publication of this report does not necessarily constitute an NRC approval of or agreement with the information contained herein.

1.0 Introduction

The Nuclear Regulatory Commission (NRC) and several State agencies have been charged with decommissioning of civilian nuclear facilities, as well as licensing and regulation of uranium mill tailings sites and commercial radioactive waste disposal facilities. The NRC and state regulators must be able to evaluate the expected performance of a decommissioned site or a waste disposal site in accordance with federal or state regulations. Current performance assessment (PA) models of radionuclide transport in soil and groundwater use simplified conceptual models for radionuclide retardation that are based on linear and reversible partition coefficients (K_D s) measured for a specific set of experimental conditions. The K_D approach should be appropriate when the site is well characterized, both chemically and hydrologically. Unfortunately, experience shows that this empirical approach often fails to correlate with field measurements of actual radionuclide transport. The reason is that experimental K_D s have localized application and are sometimes unrealistic when considering the range of nonlinear geochemical parameters that can significantly affect radionuclide transport mechanisms and kinetics (temperature, pH, fluid composition, ionic strength, mineral structure, substrate reactivity, organic complexation, etc.). To predict radionuclide retardation over a wide range of environmental conditions that are relevant to NRC licensing concerns, it is critical to understand and model each of these effects, especially for common soil minerals. Since sorption and desorption phenomena often dominate radionuclide retardation in soils, they are probably the most important geochemical processes to model in PA codes. Once radionuclide sorption and desorption mechanisms are better understood, more appropriate retardation models can be incorporated into PA codes to allow for improved treatment of uncertainty when making estimates of dose to the public.

Transport and attenuation of radionuclides in subsurface environments are largely controlled by the geochemical interactions of dissolved aqueous waste with common oxide and silicate minerals. These minerals, which range in complexity from quartz to smectite-like clays to poor and/or well-crystalline Fe- oxides/hydroxides, are found in soils and rocks adjacent to the waste site. An understanding of the surface structure and sorptive properties of soil minerals in contact with dissolved radionuclides is fundamental to modeling metal retardation. Hydrogeochemical transport codes can accurately predict the transport and retardation of dissolved radionuclides only when there is a mechanistic understanding of the adsorption and fixation behavior of metals in near-field soils.

While theoretical models exist for modeling surface complexation, sorption, and desorption at mineral surfaces, experimental verification of those models lags, as does atomistic characterization of retardation mechanisms. This NRC project, Characterization of Retardation Mechanisms in Soils; JCN B6608, is designed to provide mechanistic and kinetic data about the sorption behavior of metals with complex mineral surfaces. Unraveling the mechanistic controls on sorption under diverse geochemical conditions is necessary to predict metal transport and retardation in soils. These data will add confidence to regulatory decisions on radionuclide transport and retardation. The regulatory objectives of this project are to provide the

NRC, state regulators, and disposal site operators with data and models describing radionuclide retardation by soil-forming minerals. Specifically, it will provide evaluation and quantification of those critical mechanisms, geochemical parameters, and kinetic data that control the retardation of radionuclides on common sorbing phases in near-field soils, principally clay minerals (kaolinite and montmorillonite) and Fe-oxides/hydroxides (ferrihydrite, hematite, and goethite).

This work is multidisciplinary in nature and will involve topographic and spectroscopic characterizations of mineral surfaces by atomic force microscopy (AFM) and nuclear magnetic resonance spectroscopy (NMR) techniques, experimental measurements of adsorption isotherms (K_D s) of Cs^+, Sr^{2+}, Ra^{2+} (using Ba^{2+} as an analog) on clay and Fe-oxyhydroxide phases, and theoretical simulations of the kaolinite mineral surface and Cs sorption onto kaolinite. This integrated investigation will provide the technically defensible methodology for evaluating radionuclide migration under diverse geochemical conditions in soil environments, especially for those sites with new contaminants or with insufficient budgets to measure local K_D s.

1.1 Background

Much of the work documented in this study is based upon our earlier metal sorption and characterization results for the first three-year grant of the NRC project (JCN B6608),[1-4] as well as recent Department of Energy/Basic Energy Sciences/Geosciences research on silicate mineral dissolution.[5-9] In this earlier work, Sandia National Laboratories initiated a comprehensive investigation (analytical, experimental, and theoretical) of alkali metal sorption onto the surface of kaolinite. This research included Cs^+ sorption measurements on silica, corundum, and kaolinite, and the NMR and X-ray photoelectron (XPS) spectroscopic characterizations of the sorption of Cs^+ onto the multiple surface and interlayer sites of clay minerals. These results demonstrated the critical role of the mineral lattice framework in controlling dissolution and leaching processes, and of the effect of secondary leach layers upon their sorption properties. Furthermore, this research demonstrated the importance of modern spectroscopic characterization of the surface of the reacting mineral phase, including chemistry, atomic structure, and bonding configurations at the surface sorption sites.

Complementary to the spectroscopic characterizations and the experimental sorption measurements are state-of-the-art empirically based molecular simulations of the interactions of a monovalent cation (Cs) sorbate with a simple clay substrate (kaolinite), using consortium software provided by Molecular Simulation Inc. (MSI) for their Catalysis and Sorption Project. The computer simulations help to evaluate experimental or analytical research results and to develop a useful strategy for future work. Our work unraveling mechanistic controls on sorption is a necessary first step to understanding the general controls on metal transport in soils. In particular, our intensive, multifocused approach to Cs sorption onto kaolinite establishes a portable framework in which to consider the binding of other radionuclides to other minerals. It also allows us to scale-up our results to predict radionuclide movement in real-world situations by using the mechanistic work to quantify the sorptive sink in site-specific scenarios. In the renewal phase of this project, we began to extend this research to other sorbate metals (Sr and Ba) and substrates (e.g., the

structurally complex smectite clays such as montmorillonite, and Fe-oxyhydroxide minerals). In this document, we report on the data obtained during the course of the entire project, recognizing that many aspects of this research are unfinished and will be addressed by a new NRC project entitled "Incorporation of Mechanistic Sorption Models in SEDSS" (JCN W6811).

2.0 Procedure

Recognizing the complex chemistry associated with characterizing and evaluating the interactions of a metal sorbate with simple and interlayer clay substrates or Fe-oxides/hydroxides, we have emphasized complementary experimental, analytical, and theoretical studies of metal sorption onto model clays and colloid minerals. We initiated a comprehensive investigation of the mechanism of alkali and alkaline earth sorption onto the surfaces of several clay and Fe-oxyhydroxide minerals. This research combines spectroscopic analyses, batch sorption, surface complexation, molecular modeling, and atomic force microscopy to characterize the mechanisms by which metals adhere to mineral surfaces. Most of the work described here is for Cs sorption onto kaolinite clay, because of the clay's relatively simple chemistry and structure. General analytical and experimental studies of cation sorption processes were performed using both natural and synthetic soil mineral samples. Natural samples include KGa-1 kaolinite ($Al_2Si_2O_5(OH)_4$ from Warren County, Georgia), SAz-1 montmorillonite (Ca-interlayer clay from Apache County, Arizona) and SWy-1 montmorillonite (Na/Ca-interlayer clay from Crook County, Wyoming).). Synthetic soil mineral samples include goethite [FeO(OH)] and ferrihydrite [$Fe_2O_3 \cdot nH_2O$]. The clay and Fe-oxide minerals were chosen to provide increasingly complex structures and sorption substrates by which the mechanism of metal sorption onto mineral surfaces might be determined. For example, kaolinite is a 1:1 layer type clay mineral composed of a tetrahedral SiO_4 layer linked to an octahedral gibbsite layer (tetrahedral-octahedral [TO] structure, see Figure 1). Montmorillonite is a complex 2:1 layer type smectite clay (TOT structure), composed of an Al-deficient octahedral sheet sandwiched between two inward-pointing SiO_4 tetrahedral sheets, where interlayer cations satisfy charge balance. Characterizations of powdered minerals and reacted samples were made using standard analytical techniques (atomic absorption [AA], direct current plasma [DCP], energy dispersive spectroscopy [EDS], inductively coupled plasma-mass spectrometry [ICP-MS], transmission electron microscopy

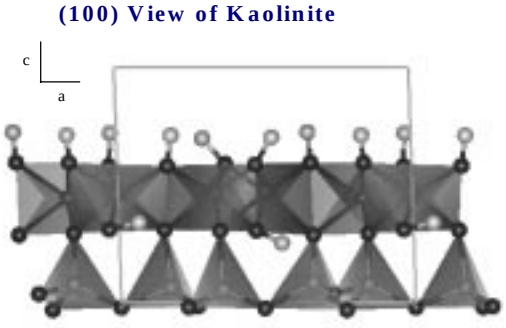

Figure 1. Schematic of kaolinite structure; note that the SiO_4 tetrahedral layer is apically bonded to a gibbsite-like octahedral layer, where the basal spacing is 7.1 Å.

[TEM], and X-ray diffractometry [XRD]) in order to verify the structure of starting materials and reacted phases, and to quantify solution compositions. Specific research procedures are described separately as tasks 1-5, which reflects the work structure of this proposal.

2.1 Task 1: Completion of characterization of Cs sorption onto kaolinite

After a series of batch Cs sorption treatments, several surface-sensitive spectroscopic techniques were used to characterize the extent and site-specific control of Cs sorption onto these minerals. These techniques included X-ray photoelectron spectroscopy, which is sensitive to the near-surface (<20 Å) composition and chemical state of elements, and nuclear magnetic resonance (NMR) spectroscopy, which yields structural and bonding information at the molecular level. In these tests, approximately 1 g of the mineral was reacted with 100 ml of 0.1 or 0.01 *M* CsCl solutions in polyethylene bottles for 5 days at 25 and 50°C. A shaking bath was used to maintain constant temperature and suspension of the sample. After the test, samples were separated by filtration. The XPS analyses were performed under vacuum (~ 2 x 10^{-9} torr) using a Perkin Elmer PHI 5400 instrument employing Mg K X-rays and a takeoff angle of 45°. Adventitious carbon (determined by the C1s binding energy) provided an internal standard for correcting energy shifts resulting from sample charging. The ^{133}Cs NMR spectra were collected at room temperature and at 65.5 mHz using a spectrometer with a 11.7-T superconducting magnet. Spectra for most samples were collected at room humidity; however, a few kaolinite and montmorillonite samples were collected at 100% relative humidity (RH) in order to evaluate interlayer site occupancy and exchange. Some samples were also cooled, or heated, in order to evaluate thermal effects upon site occupancy. The ^{133}Cs chemical shifts are reported in parts per million (ppm) relative to an external 0.1 *M* CsCl solution at room temperature.

2.2 Task 2: Computer simulations of ionic interactions with clay surfaces

A variety of computational models were utilized to simulate dissolved Cs sorption onto kaolinite surfaces. These models included lattice energy minimization, Monte Carlo, and molecular dynamics (MD). By combining all of these techniques, we have developed a general approach for evaluating sorption sites, isosteric sorption energies, docking mechanisms, and packing of the sorbates. Computer modeling results provide a fundamental basis for interpretation of analytical and experimental results. However, molecular-scale simulations of Cs sorption onto kaolinite require an accurate description of clay structures and surfaces, based either on X-ray crystal cell refinements[10] or quantum chemical structure calculations.[11] Accurate reproduction of structure and bonding in a sheet aluminosilicate mineral is necessary prior to realistic simulations of surface relaxation phenomena for the extended mineral, water, and adsorbate complex. The first all-atom geometry optimization of kaolinite has been calculated using a periodic density functional method. Since the kaolinite structure contains both interlayer OH groups that form hydrogen bonds with the adjacent silicon tetrahedral sheet and inner OH groups associated with vacant octahedral aluminum sites, it is important to include hydrogen atoms in the structure optimization. Numerous

experimental[12,13] and theoretical[11,14] studies have addressed heavy atom positions and proton orientations in kaolinite; however, no optimization calculations involving all atoms of the unit cell in a periodic structure have been conducted. Interlayer and inner OH groups also have been suggested to be significant in the surface electrostatics that influence the formation of host/guest complexes and thus may play an important role as a model in evaluating radionuclide transport.

The first-principles periodic bulk calculations used the local density approximation to density functional theory in a Gaussian-based linear combination of atomic orbitals (LCAO) basis. The calculations were performed using the QUEST (QUantum Electronic STructure) code, designed for massively-parallel, distributed-memory computer architectures. Full geometry optimization was accomplished starting with atomic coordinates from two recent refinements of X-ray and neutron diffraction.[12,13] Geometry optimizations were unconstrained for all atomic coordinates; however, experimental unit cell parameters were not adjusted relative to new atomic positions during the minimizations. All QUEST calculations were run on an 1824-processor Intel Paragon computer.

2.3 Task 3: Isothermal measurements of adsorption onto clays

Sorption isotherms for Cs^+, Sr^{2+}, and Ba^{2+} (as an analog for Ra^{2+}) onto kaolinite and smectite (montmorillonite) clays were measured as a function of temperature (25, 50, and 70°C) over a wide pH range (2-12). The titrant for the adsorption measurements was 0.1 *M* NaOH or HCl and the pH electrode was calibrated using National Institute of Standards and Technology samples at the temperature of interest. Four grams of kaolinite or montmorillonite powders (Brunauer, Emmett, and Teller [BET]) surface area ~10 m^2/g for KGa-1 and ~32 m^2/g for SWy-1) were titrated in 50 mL of 0.01-1.0 *N* $NaClO_4$ or NaCl background electrolyte solutions using a Mettler DL12 titrator. Slurries were continuously stirred and N_2 gas was pumped directly into the solution prior to and during each titration to purge CO_2 and to minimize carbonate levels in solution. Temperature was maintained by adjusting the hot plate that controlled the water bath in which the reaction vessel was immersed. Certified Cs, Sr, and Ba atomic adsorption analytic standards were diluted to parts per million (ppm) levels and used as stock solutions. Solutions containing $NaClO_4$ or $SrCl_2$ or $BaCl_2$ were used as background electrolytes in these adsorption experiments because Cl^- and ClO^-_4 do not complex with these metals strongly. Solution aliquots were taken after pH stabilization and were analyzed for metals by directly coupled plasma (DCP) or inductively coupled plasma (ICP) spectroscopy using matrix-matched standards. Metal sorption was calculated by difference from starting solutions. The dissolved metal concentrations and pH data were regressed using the computer code FITEQL[15] to calculate best-fit values of pK_x and site density for Cs, Sr, and Ba as a function of temperature.

The cation exchange capacity of SWy-1 (CEC = 76.4 mEq/100 g) is due to the permanent negative charge on the TOT layers, and it is pH-independent. This clay has a BET surface area of 31.8 m^2/g, and the primary exchangeable cations are Na^+ and Ca^{2+}.[16] Exchange equilibria onto minerals saturated with Na^+ are written as:

$$Ba^{2+} + 2{>}Na \leftrightarrow {>}Ba + 2Na^+ \quad K_{Ba} = [{>}Ba][Na+]^2/[Ba^{2+}][{>}Na]^2$$

$$Sr^{2+} + 2{>}Na \leftrightarrow {>}Sr + 2Na^{+} \quad K_{Sr} =$$

$$[{>}Sr][Na+]^2/[Sr^{2+}][{>}Na]^2$$

where ">" denotes an exchange site. The total number of exchange sites is equal to the cation exchange capacity. Bracketed terms denote concentrations here, as no effort is made at this point to correct for nonideality of the aqueous or exchange species. Note that by using Ba exchange as an example, the exchange constant K_{Ba} can be calculated at a single pH given Ba levels measured in solution from known starting points. Specifically, for the case of Ba in a 0.001*M* NaCl solution:

$$K_{Ba} = [Ba^{o} - Ba^{2+,anal}][0.001 + 2(Ba^{o} - Ba^{2+,anal})]^2/[Ba^{2+,anal}][2(CEC-(Ba^{o} - Ba^{2+,anal}))]^2$$

Ba^{o} is the spike Ba concentration (1 ppm) and $Ba^{2+,anal}$ is the analyzed Ba concentration. The equation above assumes that the surface is saturated initially with Na^{+}, and that Ba^{2+} exchanges 2:1 for Na^{+}. An analogous equation is used to calculate the exchange constant for Sr.

2.4 Task 4: AFM microcharacterization of clay surfaces

.

Metal sorption onto clay surfaces is a function of the charge distribution on the surfaces as well as the absolute proportions of exposed planes of differing surface charge. AFM studies of the starting kaolinite surface were initiated for comparison with Cs-sorbed surfaces and for characterization of exposed basal and edge crystallographic features. AFM acquisition of surface topography to the angstrom scale is based on tip/surface interaction forces, including short-range repulsive and attractive (van der Waals) forces. Relative proportions of basal and edge surface area for untreated kaolinite crystals were determined using AFM techniques. Kaolinite powder was ultrasonically suspended in water for 1 minute, after which 50 µL of this solution was placed on freshly cleaved muscovite and air dried. Images were obtained in contact mode using a Park Scientific Instruments AutoProbe LS (5 µm scanner) and 0.6 µm thick Ultralevers (silicon cantilever and tip). Scanning speeds ranged from 0.5 to 2 Hz. Particle dimensions and step heights were measured on raw images of a few representative grains. These dimensions were used to calculate relative amounts of edge and basal surface area. Estimated errors for calculated surface areas are 10% based on an averaged 5% uncertainty in a single height or length measurement. Likewise, AFM topographic images of montmorillonite were obtained with a Digital Instruments Nanoscope III using tapping mode in air with silicon tips. Montmorillonite particles were suspended in water and pipetted onto freshly cleaved muscovite for imaging. Image quality seemed to improve dramatically when the humidity was high (about 50%).

2.5 Task 5: Sorption measurements during Fe-oxide/hydroxide phase transformation

Ba sorption and desorption onto the surfaces of ferrihydrite, goethite, and hematite were measured as a function of pH, solution composition, and phase transformation. All experiments were conducted at pH 12 since earlier workers had found that high pH hastens the conversion of ferrihydrite to more crystalline products. For example, half

conversion of ferrihydrite to goethite at 25°C and pH 12 occurs in less than 4 days, while half conversion to hematite and goethite at pH 7 takes 112 days.[17] Since heating also hastens ferrihydrite transformation, our tests were conducted at 50°C using two different ionic strengths (0.01-1 *M* KNO_3) to model salt contents approaching those of fresh water and brine.

Approximately 40 g of ferrihydrite were precipitated by batch neutralization of 1 *M* $Fe(NO_3)_3$ with 1 *M* KOH to pH 8. The resulting suspension was adjusted to pH 12 and divided into two portions. Barium nitrate (0.0005 *M*) was added to one portion and then both portions were aged at 50°C. The second half of the original ferrihydrite suspension was washed free of KNO_3 by dialysis, re-suspended in 0.01 *M* KNO_3, adjusted to pH 12, and divided into 2 portions. Barium nitrate (0.0005 M) was added to one portion of the second suspension and then both portions were aged at 50°C. To measure Ba sorption or desorption on the precipitates, aliquots of the suspensions were removed periodically and centrifuged. The supernatant was passed through a 0.2 μm syringe filter and the filtrate was analyzed for Ba by DCP techniques. The precipitates from subsamples were washed and freeze dried. Iron was extracted from filtrates with 0.2 *M* ammonium oxalate and 6 *M* HCl to determine the amounts of Fe present as ferrihydrite and the total Fe content of the precipitates.[18] These extracts were also analyzed for Ba to determine the partitioning of Ba between ferrihydrite (Ba_{Ox}) and the goethite formed as the precipitates were aged (Ba_{HCl} - Ba_{Ox}). Barium adsorbed on the surface of goethite crystals may also be present in the oxalate extracts.[19] Iron and Ba in the extracts were determined by DCP. The percent transformation of ferrihydrite to goethite can be estimated from the iron analyses:

$$(1 - Fe_{Ox} / Fe_{HCl}) \times 100$$

Pressed powder mounts of the solid subsamples were analyzed by X-ray diffraction (XRD). Surface area of selected solid samples was determined by the nitrogen BET adsorption method.

3.0 Results

Results from analytical, experimental and theoretical studies of metal sorption onto common soil minerals are given in the next sections and are discussed by task.

3.1 Task 1: Completion of characterization of Cs sorption onto kaolinite

.

^{133}Cs MAS NMR and Cs XPS were used to study the adsorption of Cs on kaolinite, montmorillonite, corundum, and gibbsite from 0.1 *N* and 0.01 *N* CsCl solutions. XPS spectra for all samples except gibbsite contain strong signals associated with Cs $3d_{3/2}$ and $3d_{5/2}$ photopeaks. Peak intensity analyses of the XPS spectra indicate that powdered corundum sorbed ~0.3 mol% Cs; the kaolinite slab exhibited Cs sorption at the 1 mol% level; and powdered montmorillonite sorbed ~2 mol% Cs. Sorbed Cs concentrations were reduced by 50-75% after Ar sputtering of the near surface. Based upon these results, the relative Cs sorption capacity for these minerals is montmorillonite > kaolinite > corundum > gibbsite.

In addition to near-surface compositional profiles, XPS can measure shifts in the binding energy of core electrons resulting from a change in chemical environment (chemical shift). These shifts result from a change in the nearest neighbor, oxidation state or crystal structure. We did not observe a chemical shift for Cs sorbed onto montmorillonite nor kaolinite. Multiple surface or interlayer sites for Cs could not be resolved from the single peak Cs spectra observed for clay mineral samples (Figure 2).

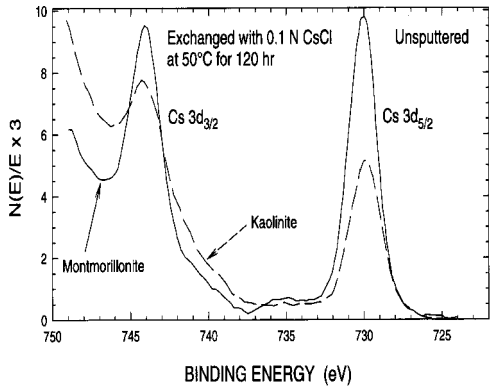

Figure 2. High-resolution XPS spectra for unsputtered kaolinite and montmorillonite after reaction with a CsCl solution; the single peaks do not identify the presence of multiple surface or interlayer sorption sites.

These same samples were also characterized by ^{133}Cs magic angle spinning (MAS)-NMR spectroscopy. There was no observed ^{133}Cs MAS-NMR spectral signal from the corundum or gibbsite samples. The NMR spectra for the montmorillonite samples contain one broad peak at -18 to -12 ppm, whereas the kaolinite samples contain multiple peaks (Figure 3), including a large, relatively narrow peak at a more shielded chemical shift (-40 to -25 ppm) along with several other weak peaks. Higher concentrations of Cs in the reacting solution,

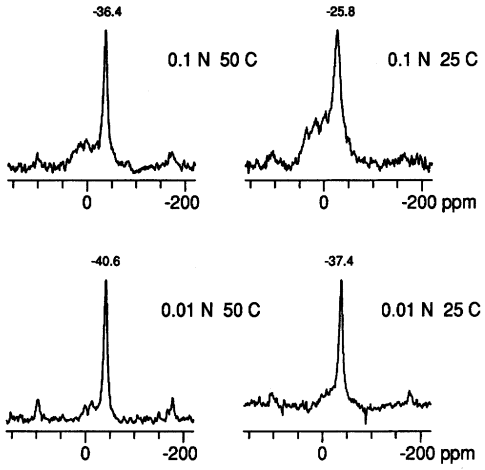

Figure 3. ^{133}Cs MAS NMR spectrum for kaolinite after reaction with CsCl solutions at 25 and 50°C; one broad and three minor peaks have been assigned to edge, surface, and 'interlayer' Cs sorption sites.

as well as lower temperatures and higher humidity, resulted in less shielded chemical shifts. There was increased peak broadening for kaolinite and montmorillonite with decreasing temperature, although separate peaks were unresolved, even at -80°C.

The ^{133}Cs NMR data, combined with TEM/XRD data for kaolinite, show that for montmorillonite most of the Cs is adsorbed in the interlayers and is motionally-averaged among two or more sites at room temperature and humidity. The spectra for kaolinite are similar to those of montmorillonite, and the tightly bonded Cs in our sample appears to be in expandable interlayers which exist as mixed layers with kaolinite, and not as discrete smectite. The Cs environments in both montmorillonite and kaolinite are sensitive to humidity. For kaolinite, the ^{133}Cs chemical shift changes at low temperature and 100% humidity, indicating that the interlayer charge of its expandable layers is very small. No ^{133}Cs NMR signal could be detected for gibbsite or corundum.

3.2 Task 2: Computer simulations of ionic interactions with clay surfaces

Symmetries of the Lattice Density Functional (LDF)-calculated kaolinite structures are consistent with the unit cell possessing overall C1 symmetry. All heavy atom positions (aluminum, silicon, and oxygen) produce an excellent mapping and reduction of the P1-based LDF structure to a C1 symmetry structure. The interlayer hydrogen positions exhibit C1 symmetry to a tolerance of 0.018 Å, whereas the inner hydrogens of kaolinite agree to within 0.064 Å. Both hydrogen position tolerances are similar to the offsets expected from the standard deviations obtained for the atomic positions from the neutron diffraction data.[12] Overall structural agreement between heavy atoms and protons of the energy-optimized structure and recent refinement is excellent. Bond lengths and bond angles (see Figure 4) are generally consistent with what has been found for other clays, kaolinite[12] and dickite.[20] Differences in O-H bond distances are also found for the inner and interlayer OH groups, and are on the order of 0.01 Å. Hydroxyl group orientations in the geometry-optimized

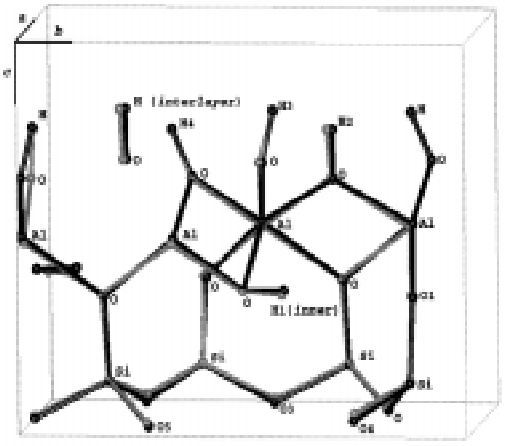

Figure 4. Comparisons of calculated (dark) and experimental (light) kaolinite structures.

structures are also similar to those determined through model fitting of the neutron diffraction data. Only minor differences in bond angles (less than 0.5°) were observed between the full- and hydrogen-only optimized structures. Moreover, the two inner OH positions of the P1 symmetry unit cell used for all calculations are identical.

Comparisons of the calculated neutron powder diffraction intensities, based upon coordinates from the energy-optimized and

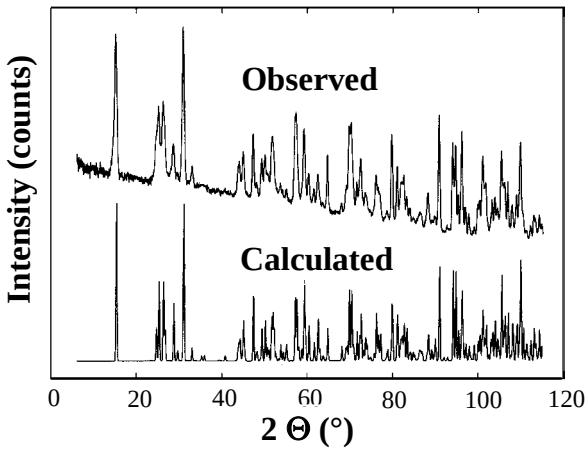

Figure 5. Neutron powder diffraction patterns for Keokuk kaolinite (observed) and that calculated for an LDF-optimized structure.

observed structures, are in excellent agreement (Figure 5). The calculated diffraction pattern for kaolinite was generated from the unit cell obtained for the all-atom LDF optimization. All major and almost all minor peak positions and their relative intensities are comparable for both structures. In a similar fashion, we examined the X-ray diffraction pattern associated with the LDF-based structure. No C1-violating peaks were observed at 9.9° and within the 15.5° to 19.0° 2θ range. These results support earlier conclusions[12] that the kaolinite structure can be characterized by a crystal lattice that is nonprimitive and

possesses C-centering. Most convincing in these results is that our LDF calculations were performed on a unit cell with P1 symmetry (no unit cell symmetry) that ultimately energy optimizes (regularizes) to the more symmetrical C1 unit cell.

Molecular electrostatic potential (MEP) calculations, which represent the net summation of the atomic partial charges at the mineral cluster surface, were performed using the observed crystallographic structure of kaolinite[5] and energy minimized positions for hydroxyl groups on selected surfaces. The MEP surface (Figure 6) depicts the most favorable sites for ionic sorption on kaolinite. MEP results show that there is a significant

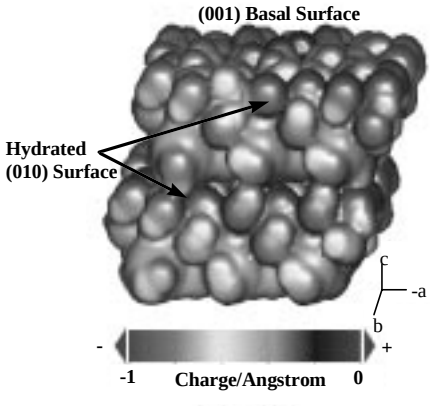

Figure 6. Molecular electrostatic potential surface of hydrated kaolinite crystal viewed along (010) edge; arrows point to areas of high negative charge.

difference in the electrostatic potential of edge and basal surface sites.[21] That is, siloxane and gibbsite basal planes (001) are not as negatively charged as edge silanol or aluminol edge sites, and are more reactive for cation sorption (greater negative electrostatic charge) than the edge silanol sites.

Both energy minimization and molecular dynamics techniques were used to simulate the interactions of dissolved cesium with a kaolinite surface. One Cs^+ atom, along with its waters of hydration, was positioned adjacent to either the (010) edge or the (001) basal aluminol surface of kaolinite prior to energy minimization. Simulations indicate that Cs^+ sorbs directly to the aluminol ((010) edge) as an inner sphere complex (Figure 7). Note that the solvating water

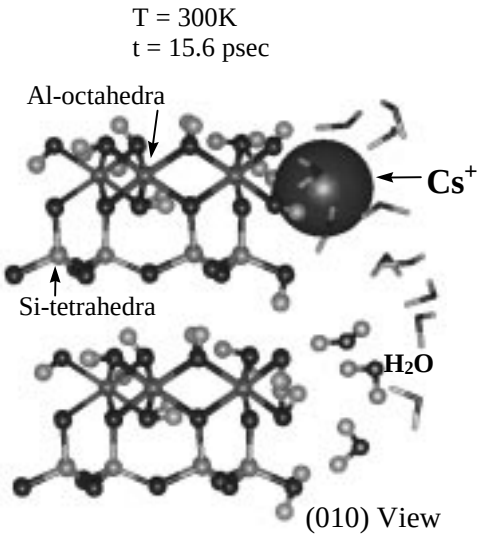

Figure 7. MD Simulation of inner-sphere sorption of Cs^+ ion onto aluminol site at (010) edge of the kaolinite structure.

molecules are not positioned between the Cs^+ and the (010) edge of kaolinite, but rather coordinate to silanol and other unreacted edge sites. Energy minimization results for the (001) surface indicate that Cs^+ is coordinated to the basal aluminol plane as an outer sphere complex, with waters of hydration completely surrounding the Cs^+. This contrasts sharply with the inner sphere configuration of Cs^+ sorption at the (010) edge.

However, shortly after equilibration of the water molecules on the (001) surface, Cs^+ (outer sphere complex) migrates toward the (010) edge and repositions itself as a an inner sphere complex coordinated to an

aluminol site. Clearly, these computer simulations suggest that the edge aluminol site is the preferred Cs^+ sorption site on a stoichiometric kaolinite.

3.3 Task 3. Isothermal adsorption measurements onto clays

Potentiometric surface charge titrations were made with quartz, corundum, and kaolinite slurries at 25 and 50°C to evaluate the pH dependence of multisite surface charge as a function of temperature.[21] Proton donor-acceptor reactions were found to occur simultaneously on the Si and Al sites exposed at basal planes and edges. We found that the Si site acidity at the kaolinite-solution interface differs minimally from that of pure SiO_2, whereas Al sites became appreciably more acidic with substitution into the kaolinite matrix. Increasing temperature causes both Al and Si sites to become more acidic, the Si sites more so than the Al sites. Calculated site densities increase with increasing temperature, suggesting appreciable surface roughening. The combination of increasing site acidity and density points to kaolinite having a greater sorptive potential at higher temperatures. Measured Cs^+ sorption isotherms onto kaolinite surfaces at 25°C and in three background electrolyte solutions (0.01-1.0 *M* NaCl) are shown in Figure 8. These titrations were conducted from low to high pH and then reversed from high to low pH. At each ionic strength (IS), there is clear hysteresis in the sorption behavior. Cs^+ is irreversibly sorbed by kaolinite, particularly at pH <6. In addition, we see that as the IS of Na^+ increases by 2 orders of magnitude, the sorbed Cs^+ decreases by about an order of magnitude and that the absolute concentration of Na^+ is 5-6 orders of magnitude greater than that of Cs^+.

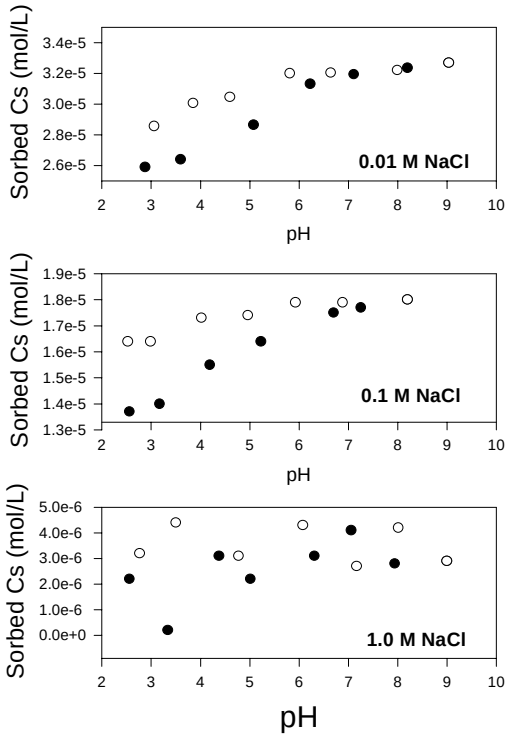

Figure 8. Sorption (filled circles) and desorption (open circles) of Cs^+ onto kaolinite as a function of ionic strength at 25°C.

We hypothesize that irreversibly-sorbed Cs^+ is associated with the siloxane basal surface, which might have a small pH-independent residual charge. However, the slight but tangible pH dependence of Cs^+ sorption at all ionic strengths suggests that some sorbed Cs^+ is also associated with edge sites (probably aluminols) that possess a pH-dependent charge. Sorption isotherms for Sr^{2+} and Ba^{2+} onto kaolinite surfaces at 25°C are shown in Figure 9, where >Me denotes sorbed metal and the solid line is a best fit using a constant capacitance surface complexation model. Note that at a given pH, the relative binding strength of Ba^{2+} to kaolinite is significantly stronger than that measured for Sr^{2+} (pK_{Sr} = 6.44 vs. pK_{Ba} = 6.02). Both metals demonstrate the same pH-dependent sorption isotherm at high pH, but significant pH-independent sorption

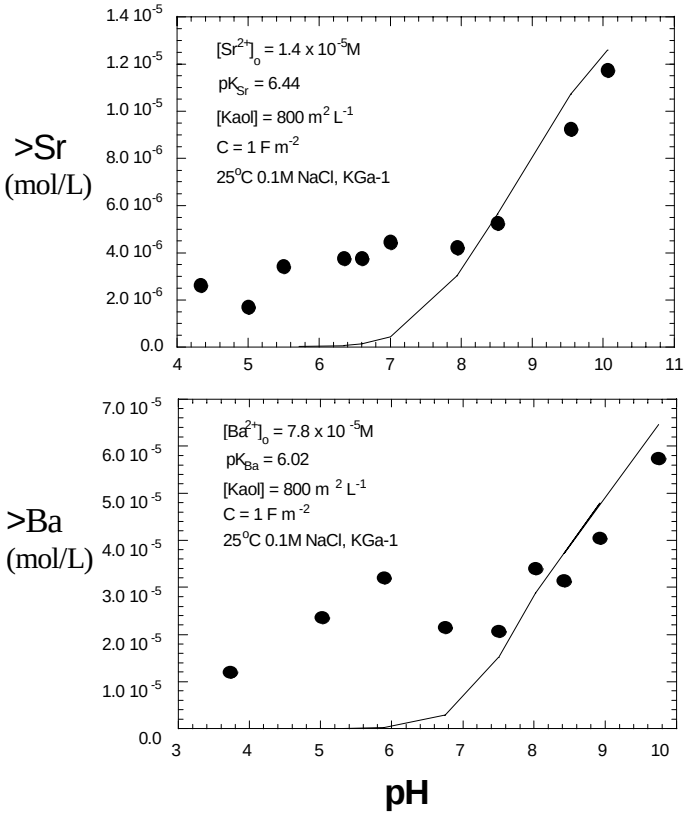

Figure 9. Sorption isotherms for Sr and Ba onto kaolinite; the line is best fit for the constant capacitance surface complexation model.

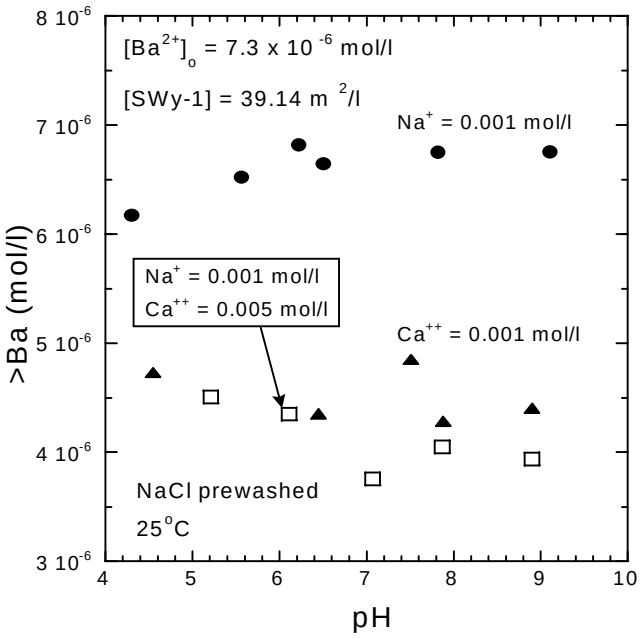

Figure 10. Ba sorption on Swy-1 (pretreated with NaCl to remove exchangeable Ca) at 25°C as a function of solution pH and Ca/Na ratio.

occurs in acid solutions (pH<7). The most likely explanation is that metal binding in acid solutions occurs at the basal siloxane layer because of a small permanent and pH-independent charge arising from minor substitution of Al^{3+} and/or Fe^{3+} for tetrahedral Si^{4+}. Figure 10 shows the amount of Ba exchanged onto prewashed SWy-1 as a function of pH and the Ca/Na ratio of the solution. Table 1 lists the calculated constant for Ba/Na exchange as a function of pH in 0.001*M* NaCl solutions. Note that the exchange constant is relatively independent of pH, suggesting that sorption onto edge sites is minor. Note that adding Ca^{2+} to the solution decreases the amount of Ba exchanged onto the clay. Millimolar levels of Ca^{2+} decrease Ba retention by about 40%. Again, there is no clear pH dependence observed in the retention of Ba.

Table 1. Ba/Na Exchange Constants

pH	K_{Ba}
4.3	2.3
6.2	6.0
6.5	4.3
7.8	5.2
9.1	5.3

Figures 11 and 12 show Ba and Sr exchange onto Swy-1 that was not washed or presaturated with Na^{+}. Instead, the basal planes probably possessed both Ca and Na as opposed to just Na^{+}. The same trends are noted as in the Na-saturated case; i.e., metal sorption (via exchange) is independent of pH, and Ca suppresses exchange. The only exception to this behavior appears to be Sr

exchange at pH > 7, where appreciable desorption occurs.

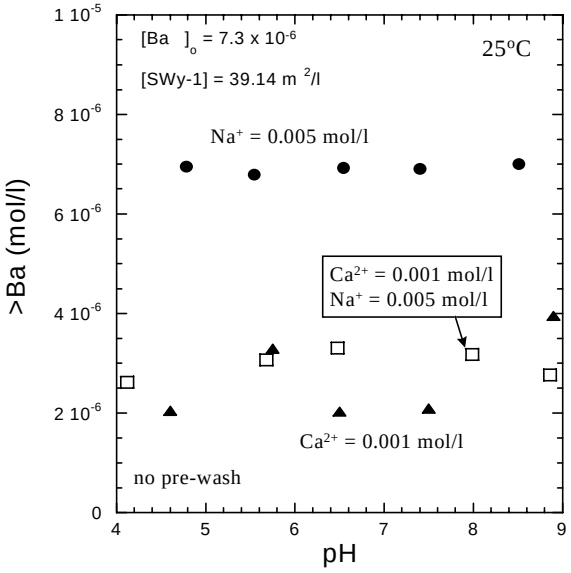

Figure 11. Ba exchange onto unwashed SWy-1.

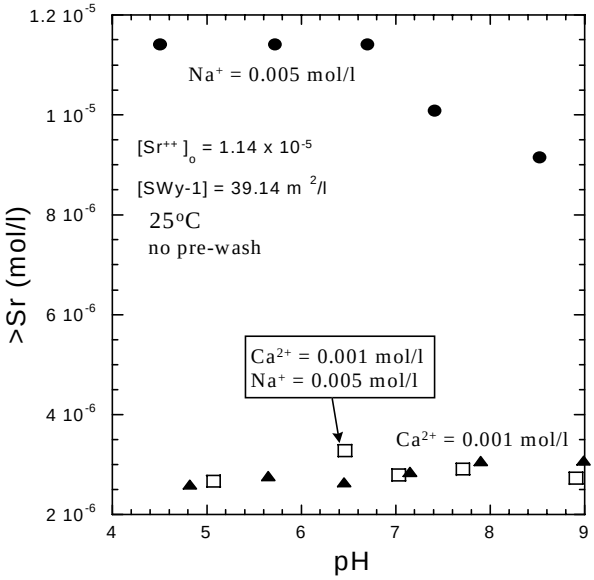

Figure 12. Sr (lower) exchange on unwashed SWy-1.

3.4 Task 4: AFM microcharacterization of clay surfaces

Images of KGa1 kaolinite were obtained using contact-mode AFM in air, where reported particle dimensions were based on images of only 7 discrete particles (Figure 13). More images were not acquired because of the difficulty of mounting the kaolinite on mica surfaces and imaging via contact mode in air. Practical experience has shown that the exceptionally low humidity of Albuquerque, NM (~15%) makes imaging small particles in air even more difficult. Particles of untreated kaolinite range from 0.1 to 0.8 µm in diameter and 100 to 1200 Å in total thickness (average 7-8 unit cells in height; see Figure 13). Assuming particles are hexagonal in shape and that similar steps occur on both basal surfaces, we estimate that edge-to-basal surface area ratios range from 15 to 50%. Edge surface areas were estimated from small steps on the clay surface (Figure 13b), and are typically 1 to 10 unit cells high (7 to 70 Å). They increase the edge surface area obtained from the gross shape of the grain by a minimum of 10%. The additional contribution of step edge area depends on the

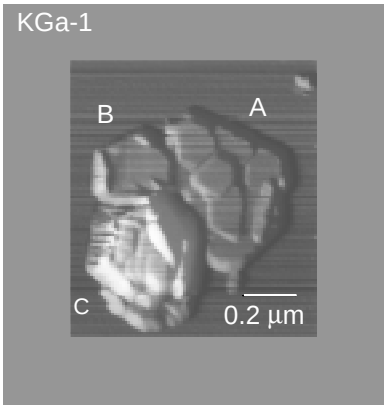

Figure 13. AFM image of kaolinite crystallites (001) orientation, with well-developed hexagonal habit; upper right crystal has surface steps of ~800 Å in height.

Figure 14. Tapping mode AFM image of Swy-1 montmorillonite; particle size ranges from 0.1-1 μm.

number and average height of the steps. The potentiometric titration results require a site density of 2.25 sites/nm^2 to explain the amount of adsorption assuming that the entire BET surface area sorbs hydrogen or hydroxyl ions. Crystallographic site densities are estimated to be 3 to 6 sites/nm^2. Therefore, if adsorption occurs only at edge sites where the density of charged sites is highest, a minimum of 38% of the BET surface area must be edge surface. This amount of edge surface is approximately the median of the range gleaned from limited AFM observations. Recent measurements of particle dimensions and surface morphologies of 150 grains of KGa-1 kaolinite led to the same conclusions as ours. In terms of particle statistics, this confirms earlier work on fibrous illites[22] where the mean particle thickness was the same for 13 or 60 particles, although particle size distribution was more statistically significant for the larger sample size. The particle morphology of SWy-1 montmorillonite also was measured by AFM techniques (Figure 14). This sample of montmorillonite contains trace quartz and calcite. Its BET surface area, measured using N_2(g), is 31.82 m^2/g. Montmorillonite particles range in diameter from a minimum of about 0.1 μm to a maximum of about 1 μm, and particle thickness ranges from about 2 to 45 nm. The thicker particles appear to be composed of overlapping thinner particles 20 to 30 nm thick. The thin particles are also extremely flat on their basal surfaces. Aspect ratio (thickness to diameter) ranges from about 0.02 to 0.45. Edge surface area ranges from 4 to 9%, much less than that observed for the KGa-1 kaolinite. This percentage of edge surface area is more in line with values typically estimated for clays. Most particles appear irregular in outline with minimal basal surface topography (i.e., rare unit-cell high steps). Although samples were sonicated for only 20-30 sec in an ultrasonic bath, it is possible that some cleavage and breakage occurred, particularly in the case of the smaller, thinner particles.

3.5 Task 5: Sorption measurements during Fe-oxide/hydroxide phase transformation

Barium sorption data from the ferrihydrite transformation experiment at pH 12 and 50°C in 0.01 *M* KNO_3 with Ba added are presented in Figure 15. Analyses of the suspension filtrate indicate that 100% of the Ba added was retained by the iron oxide for at least 25.2 h of aging and that 4 and 7% of the Ba was desorbed after 45.9 and 68.4 h of aging, respectively. Barium desorption began when ferrihydrite transformation to goethite was 92 to 94% complete. Consequently, the amount of Ba sorbed by ferrihydrite (Ba_{Ox}) began to decrease after

25.2 h of aging. The Ba sorbed by goethite (Ba_{HCl} - Ba_{Ox}) increased at the beginning of the aging period (0.4 to 19.3 h) and then remained constant as ferrihydrite

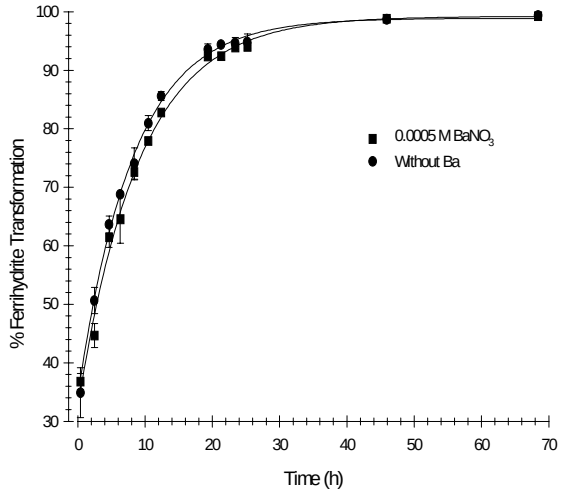

Figure 15. Percent transformation [(1-Fe_{Ox}/Fe_{HCl} X 100] of ferrihydrite aged in 0.01 *M* KNO_3 at pH12 and 50°C.

transformation neared completion.

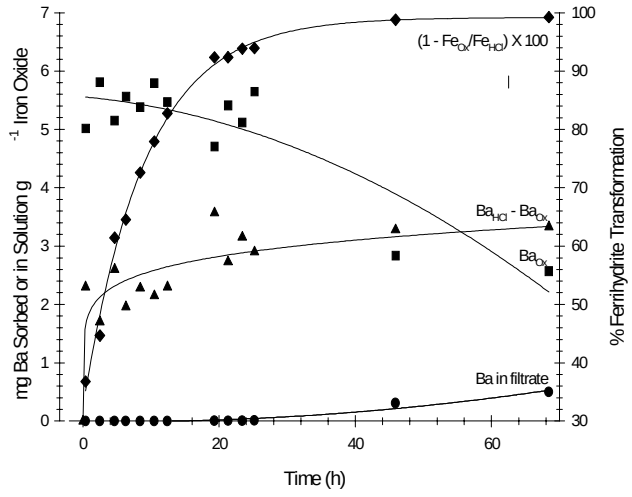

Figure 16. Ba sorption on ferrihydrite at pH 12 and 50°C; note the transformation of ferrihydrite to goethite with time and the associated drop in Ba sorption.

Figure 16 compares the percent transformation of ferrihydrite for samples aged at 50 °C in 0.01 *M* KNO_3 with and without Ba. Although this graph shows a slight decrease in transformation rate in samples with Ba added during the first 12.4 h of aging, the decrease is not consistently greater than the standard error of the data. After 25.2 h of aging, there is no difference between the rate of ferrihydrite transformation with and without Ba. Other workers have found that cation sorption may retard ferrihydrite transformation.[19, 23-25] The very slight decrease in transformation rate indicates that addition of 0.0005 *M* Ba was not sufficient to prevent ferrihydrite dissolution or goethite nucleation and crystal growth.

Figure 17 displays XRD patterns for subsamples taken during 68.4 h of aging without Ba at 50°C in 0.01 M KNO_3, while the XRD patterns of subsamples aged with Ba during the same time period are shown in

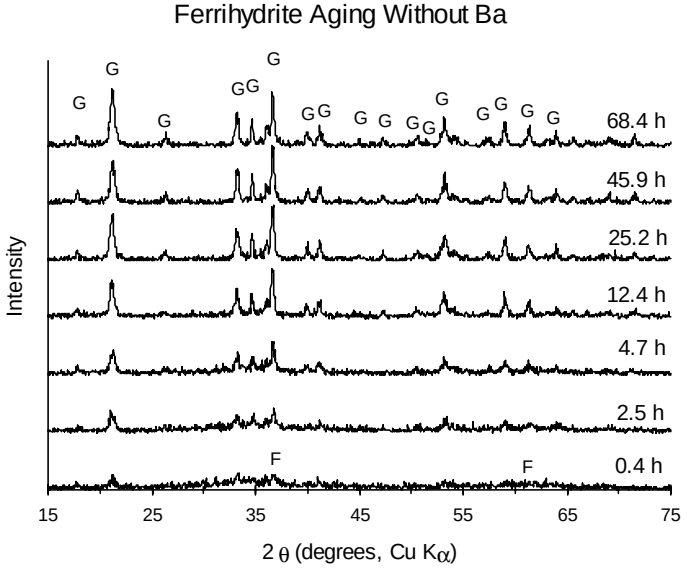

Figure 17. XRD patterns of ferrihydrite samples aged in 0.01 *M* KNO_3 at pH12 and 50°C (F=ferrihydrite; G= goethite).

Figure 18. These data also show a slight

decrease in transformation rate in samples with Ba added during the first 12.4 h of aging. No difference can be detected in this study between XRD patterns for samples aged with or without Ba from 12.4 to 68.4 h .

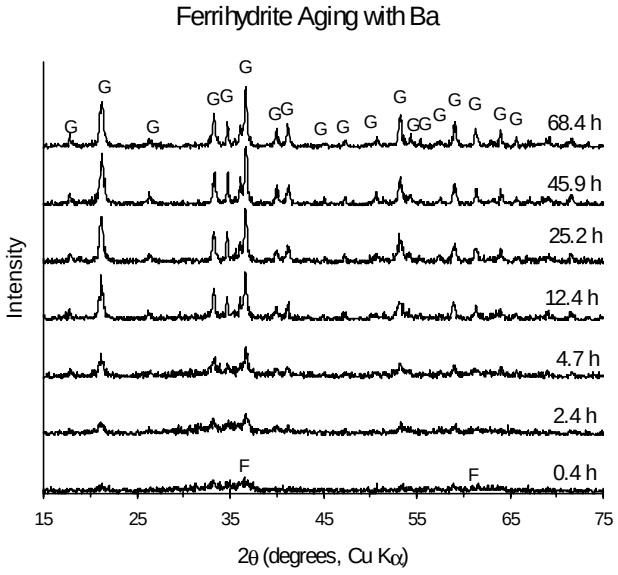

Figure 18. XRD patterns of ferrihydrite samples aged in 0.01 *M* KNO_3 and 0.0005 *M* $BaNO_3$ at pH12 and 50°C (F = ferrihydrite; G = goethite).

Figures 17 and 18 show that some poorly crystalline goethite formed during the first 0.4 h of aging and that the goethite XRD peaks increase in intensity and decrease in width during the first 12.4 h of aging. This indicates an increase in the amount of goethite present and its crystallinity. Between 12.4 h and 25.2 h of aging, there are no further changes in XRD peak width and a slight increase in peak height, indicating an increase in the amount of crystalline goethite present. After 25.2 h of aging, when the transformation of ferrihydrite to goethite is 94 to 95% complete (Figure 16), there are no further changes in the XRD patterns of the samples. Figure 15 also shows that the amount of Ba partitioned to goethite (Ba_{HCl} - Ba_{Ox}) appears to reach a constant level after about 25.2 h.

Figure 19 displays changes in surface area of these samples during aging. The surface

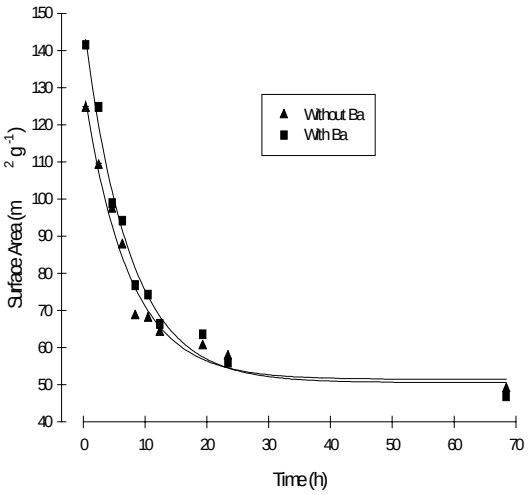

Figure 19. BET surface areas of ferrifydrite aged at 50°C and pH12 in 0.01 M KNO_3.

area of samples aged with and without Ba decreased rapidly during the first 19.3 h of aging and then approached a constant level. The surface area decreased rapidly until the transformation of ferrihydrite to goethite neared completion (Figure 16). Barium desorption may be caused by this decrease in surface area. The surface areas of samples aged without Ba appear to be slightly lower than those of samples aged for the same time with Ba during the first 19.3 h of the experiment.

In the pH range of 6 to 10, Ba is known to sorb on ferrihydrite[26] and sorbs more strongly at pH values above its zero point of charge (pH > 8). Goethite is thought to form from ferrihydrite by dissolution and reprecipitation.[27] Although Ba^{2+} is too large to replace Fe(III) in the goethite structure, Ba released after ferrihydrite dissolution

may have been adsorbed and then occluded during rapid nucleation of goethite crystals. As the goethite crystals grew larger, surface area decreased and the number of sites for Ba sorption and/or occlusion also decreased, causing some Ba to be desorbed. Future experiments with longer aging periods will determine whether Ba desorption reaches a constant level or ceases with time. In particular, atomic force microscopy will be used to relate ferrihydrite aging with and without Ba to changes in crystal size and morphology. Initial trends indicate that Ba may slow the transformation of ferrihydrite to goethite.

4.0 Discussion

One of the primary goals of this study is to identify specific sites and mechanisms for metal sorption, as well as to quantify the kinetics and magnitude of alkali or alkaline earth sorption and desorption on clay and Fe-oxyhydroxide minerals. XPS analyses of Cs-reacted clay minerals suggest that Cs is sorbed on montmorillonite and possibly on kaolinite, although the spectral resolution of XPS analyses is insufficient to differentiate among basal, edge, or interlayer sites. ^{133}Cs MAS- NMR results demonstrate that Cs is adsorbed in a motionally averaged interlayer site of montmorillonite. NMR spectra for the kaolinite samples, however, show the presence of as many as four distinct sites. The bulk of these sites is thought to consist of edge and basal plane sites, in addition to some smectite-like "exchangeable interlayer" sites. The latter probably result from the presence of small quantities of smectite-like layers on the kaolinite crystallites. Given the sheet-like structure of kaolinite, exposed Si and Al sites at the crystal's edge would provide likely sorption sites suggested by the ^{133}Cs NMR spectra. It is not surprising that the NMR results for montmorillonite indicate a continuum of Cs sorption sites, given the basal plane interlayer exchange capacity of smectite.

Metal sorption onto clay surfaces is a function of the charge distribution on the surfaces as well as the absolute proportions of exposed planes of differing surface charge. Although total surface areas can be measured using routine BET methods, the best way to determine proportions of edge and basal surfaces is to use an imaging technique in which all three dimensions can be determined on individual particles (e.g., AFM).[25] Quantification by AFM of edge and basal surface areas for kaolinite showed that edges can comprise as much as 50% of the total BET surface area. This is in contrast to untreated SWy-1 montmorillonite, where edge surface areas typically measure <10%, much less than that observed for the KGa-1 kaolinite. This percentage of edge surface area for smectite clays is more in line with values typically estimated for clays. Obviously, better statistical characterization of surface area proportions for a variety of clays and other fine-grained soil phases could significantly affect the interpretation of both spectroscopic and experimental sorption data. However, it is apparent that the decreased grain size and thinner clay platelets of the montmorillonite sample result in increased surface area and available basal reactive sites. In addition, smectites have very reactive basal surface sites due to heterovalent octahedral and tetrahedral lattice substitutions, which induce a permanent charge to the (001) surfaces.

Surface complexation modeling of proton potentiometric measurements of kaolinite and its component oxides suggest that metal binding on clay minerals occurs on multiple sites. Of the four sites indicated by the NMR work, only two dominate the overall sorptive capacity of kaolinite. The surface charge and metal sorption properties of kaolinite were found to be largely pH dependent, reflecting the acid-base properties of constituent Si- and Al-oxide and hydroxides. Regressed surface charge equilibrium constants and site

densities for KGa1, using a multisite reactivity model (both Al and Si on edge and basal plane sites), suggest that either the siloxane basal plane plays a greater role in overall surface charge than would be expected for fully satisfied siloxane bonds or that the number of pH dependent edge sites is underestimated.[21] However, AFM studies of KGa1 particle surfaces have shown that up to 50% of kaolinite edges sites are exposed,[21] where most of the KGa1 surface charge is attributed to a combination of exposed Al- and Si-sites on the basal plane and edges without calling upon proton sorption or desorption from the siloxane basal plane. This is consistent with an interpretation of H^+/OH^- adsorption occurring primarily at charged edge sites, and by implication, with metal sorption also occurring primarily at edge sites. However, multivalent octahedral and tetrahedral cationic substitutions that commonly give rise to the compositional and surface charge variability of expandable TOT layer clays (smectites) will probably pose special problems when predicting metal sorption properties.

In order to simulate, at an atomistic level, specific site acidity at edge and basal plane sites in kaolinite and metal sorption reactions, clay structures for realistic compositions need to be ascertained either from experimental diffraction, or ab initio simulation techniques. For the first time, the structural features of kaolinite have been accurately predicted by LDF molecular orbital methods, including the general C-centering and C1 symmetry in the pure crystal as well as the hydroxyl orientations in the interlayer region.[12] Further, the calculated O-H bond lengths and hydrogen bonds correlate well with observed single-crystal infrared spectra of kaolinite.[28] Empirical MD simulations suggest that Cs^+ is sorbed on kaolinite at aluminol (010) edge sites as an inner-sphere complex and weakly sorbed as an outer-sphere complex on (001) basal surfaces. These computer simulations are consistent with results of sorption and desorption isotherms as a function of ionic strength. MEP calculations also show that there is a significant difference in the electrostatic potential of kaolinite edge and basal surface sites,[21] where siloxane and gibbsite basal planes (001) are not as negatively charged as edge silanol or aluminol sites (010), and aluminol edge sites have greater negative electrostatic charge than edge silanol sites. The combination of charge distributions calculated from potentiometric titrations, proportions of edge and basal plane areas measured from AFM images, and MEP surface charge densities calculated from atomistic simulations provides a consistent picture of distinct crystallographic sites that control kaolinite surface charge and reactivity. That is, aluminol edge sites are preferred metal sorption sites over edge silanol or basal Si- or Al-sites. It should be noted that a small permanent negative charge may exist on the basal planes due to ionic substitutions in the octahedral or tetrahedral layers.

Relative metal binding strengths over all kaolinite sites were found to decrease from Ba^{2+} to Sr^{2+} to Cs^+, where metals are sorbed on both kaolinite edges and basal surfaces. Some fraction of these metals also appears to be irreversibly sorbed and cannot be easily desorbed from the kaolinite surface. For unwashed montmorillonite, the relative binding strength for Ba is slightly greater than that for Sr. Also for montmorillonite, metal sorption appears to occur via a simple exchange reaction and is independent of pH; the presence of Ca in solution seems to suppress cation exchange. The only exception to the pH-independent metal sorption behavior appears to be Sr exchange at pH > 7, where appreciable desorption occurs. The Sr behavior is anomalous, and

we do not at present have an explanation for it.

Barium is known to sorb on ferrihydrite in the pH range of 6 to 10 and sorbs more strongly at pH values above its zero point of charge (pH > 8).[24] Goethite is thought to form from ferrihydrite by dissolution and reprecipitation.[25] Although Ba^{2+} is too large to replace Fe(III) in the goethite structure, Ba released after ferrihydrite dissolution may have been adsorbed and then occluded during rapid nucleation of goethite crystals. As the goethite crystals grew larger, surface area decreased and the number of sites for Ba sorption and/or occlusion also decreased causing some Ba to be desorbed. Future experiments with longer aging periods will determine whether Ba desorption reaches a constant level or ceases with time. In particular, atomic force microscopy will be used to relate ferrihydrite aging with and without Ba to changes in crystal size and morphology. Initial trends indicate that Ba may slow the transformation of ferrihydrite to goethite.

5.0 Conclusions

A combination of analytical, experimental and theoretical techniques was used to characterize the sorption mechanism for Cs^{+}, Ba^{2+}, and Sr^{2+} onto several common soil minerals, including kaolinite and montmorillonite clays as well as goethite and ferrihydrite Fe-oxyhydroxide phases. Most of these efforts were devoted to a mechanistic understanding of Cs sorption onto kaolinite, and provide a basis for understanding and predicting metal sorption onto simple clays and a general framework for characterizing the sorption of other metals onto more complex soil minerals. Sorption models describing surface complexation reactions are based on measured adsorption isotherms, bulk solution-mineral surface complexation reactions, and molecular or atomistic models of the mineral-solution interface. Care clearly should be exercised when applying these preliminary models to contaminated sites because they are only a hypothetical interpretation of metal sorption in very complex systems and are undoubtedly, affected by multiple physicochemical processes.

6.0 References

1. Kim, Y., Cygan, R. T., and Kirkpatrick, R. J., ^{133}Cs NMR and XPS investigation of Cs adsorbed on clay minerals and related phases, *Geochimica et Cosmochimica Acta*, 60, 1041-1052, 1996.
2. Kim Y., Kirkpatrick, R. J. and Cygan, R. T., ^{133}Cs NMR Study of Cs on the Surfaces of Kaolinite and Illite, *Geochimica et Cosmochimica Acta*, 60, 4059-4074, 1996.
3. Kim, Y., Kirkpatrick, R. J., and Cygan, R. T., ^{133}Cs NMR study of Cs reaction with clay minerals, In R. A. Palmer and V. Jain, Eds., *Environmental Issues and Waste Management Technologies in Ceramic and Nuclear Industry*, Am. Ceramic Soc., Columbus, 629-636, 1995.
4. Westrich, H. R., Cygan, R. T., Brady, P. V., Nagy, K. L., Anderson, H. L., Kim, Y., and Kirkpatrick, R. J., The sorption behavior of Cs and Cd onto oxide and clay surfaces, In *Proceedings of the Waste Management Conference, WM'95*, 24-4, 1995.
5. Brady P. V., Silica surface chemistry at elevated temperatures, *Geochimica et Cosmochimica Acta*, 56, 2941-2946, 1992.
6. Brady P. V., Alumina surface chemistry at 25, 35, and 60 C, *Geochimica et Cosmochimica Acta*, 58, 1213-1217, 1994.
7. Casey, W. H., Westrich, H. R., Banfield, J. F., Ferruzzi, G., and Arnold, G. W., Leaching and reconstruction at the surfaces of dissolving chain-silicate minerals, *Nature*, 366, 253-256, 1993.
8. Nagy, K. L., Dissolution and precipitation kinetics of sheet silicates, In *Chemical Weathering Rates of Silicate Minerals*, Reviews in Mineralogy Vol. 31, Mineral. Soc. Am., 173-233, 1995.
9. Westrich, H. R., Cygan, R. T., Arnold, G. W., Zemitis, C., and Casey, W. H., The dissolution kinetics of mixed-cation orthosilicate minerals, *Am. Journal of Sci.*, 293, 1-25, 1993.
10. Bish, D. L. and Von Dreele, R. B., Rietveld refinement of non-hydrogen atomic positions in kaolinite, *Clays and Clay Minerals*, 37, 289-296, 1989.
11. Hess, A. C. and Saunders, V. R., Periodic ab initio Hartree-Fock calculations of the low-symmetry mineral kaolinite, *Journal of Physical Chemistry*, 96, 4367-4374, 1992.
12. Bish, D. L., Rietveld refinement of the kaolinite structure at 1.5 K, *Clays and Clay Minerals*, 41, 738-744, 1993.
13. Young, R. A. and Hewat, A. W., Verification of the triclinic crystal structure of kaolinite, *Clays and Clay Minerals*, 36, 225-232, 1988.
14. Giese, R. F. and Datta, P., Hydroxyl orientations in kaolinite, dickite, and nacrite, *American Mineralogist*, 58, 471-479, 1973.
15. Westall, J. C., *FITEQL - A computer program for determination of chemical equilibrium constants from experimental data*, Report 82-02, Dept. of Chemistry, Oregon State University, Corvalis, OR, 1982.

16. Van Olphen, H., and J. J. Fripiat, *Data Handbook for Clay Materials and other Non-Metallic Minerals*, Pergamon Press, New York, 1979.

17. Schwertmann, U., and Murad, E., The effect of pH on the formation of goethite and hematite from ferrihydrite, *Clays and Clay Minerals*, 31, 277-284, 1983.

18. Schwertmann, U., Differenzierung der eisenoxide des bodens durch extraktion mit ammoniumoxalat-lösung, *Z. Pflanzenernähr. Bodenkd.*, 105, 194-202, 1964.

19. Cornell, R.M., The influence of some divalent cations on the transformation of ferrihydrite to more crystalline products., *Clays and Clay Minerals*, 23, 329-332, 1988.

20. Bish, D. L. and Johnston, C. T., Rietveld refinement and Fourier-transform infrared spectroscopic study of the dickite structure at low temperature, Clays and Clay Minerals, 41, 297-304, 1993.

21. Brady P. V., Cygan, R. T., and Nagy, K. L., Molecular controls on kaolinite surface charge, *Journal of Colloid and Interface Science*, 183, 356-364, 1996.

22. Nagy, K. L., Application of morphological data obtained using scanning force microscopy to quantification of fibrous illite growth rates, In *Scanning Probe Microscopy of Clay Minerals*, K. L. Nagy and A. E. Blum, Eds., *The Clay Minerals Society Workshop Lectures*, Vol. 7, pp. 203-239, 1994.

23. Axe, L., and Anderson, P. R., Sr diffusion and reaction within Fe oxides: Evaluation of the rate-limiting mechanism for sorption, *Journal of Colloid and Interface Science*,175, 157-165, 1995.

24. Baltpurvins, K.A., Burns, R.C., Lawrance, G. A., and Stuart, A. D., Effect of Ca^{2+}, Mg^{2+}, and anion type on the aging of iron (III) hydroxide precipitates, *Environmental Science and Technology*, 31, 1024-1032, 1997.

25. Ford, R.G., Bertsch, P.M., and Farley, K.J., Changes in transition and heavy metal partitioning during hydrous iron oxide aging, *Environmental Science and Technology*, 31, 2028-2033, 1997.

26. Kinniburgh, D.G., Jackson, M. L., and Syers, J.K., Adsorption of alkaline earth, transition, and heavy metal cations by hydrous oxide gels of iron and aluminum, *Soil Science Society of America Journal*, 40, 796-799, 1976.

27. Schwertmann. U., and Fischer, W., Zur Bildung von α-FeOOH und α-Fe_2O_3 aus amorphem Eisen(III) hydroxide, *Z. Anorg. Allg. Chem.*, 346, 137-142, 1966.

28. Johnston, C. T., Agnew, S. F., and Bish, D. L., Polarized single-crystal Fourier-transform infrared microscopy of Ouray dickite and Keokuk kaolinite, *Clays and Clay Minerals*, 38, 573-583, 1990.